Settling Properties of Asphaltene Aggregates

Nazmul H. G. Rahmani,[†] Tadeusz Dabros,[‡] and Jacob H. Masliyah*,[†]

Department of Chemical and Materials Engineering, University of Alberta, Edmonton, Alberta, Canada T6G 2G6, and CANMET, Devon, Alberta, Canada T9G 1A8

Received December 17, 2004. Revised Manuscript Received March 11, 2005

Stokes law is the fundamental equation to describe the settling velocity of a particle for small Reynolds number flow and is applicable when the particle is spherical and impermeable. However, this equation is not suitable to describe the settling of porous aggregates found in many industrial applications, because of the nonsphericity and flow through the pores of the aggregates. Free-settling tests were used in the present work to estimate asphaltene aggregates porosity and effective density. The settling velocities of individual asphaltene aggregates are measured in a quiescent column via a photographic technique. Data analysis was conducted with a video frame grabber and digital imaging software, to determine the particle size, shape, and settling velocity. Results show that the aggregate size (area-equivalent diameter) determined from the video images ranged from 20 μm to 200 μm and the measured settling velocities varied from 100 μm/s to 564 μm/s. Settling velocity measurements indicated an inverse relationship between aggregate size and density. The reduced aggregate density with increasing size was attributed to the entrainment of fluid into the aggregate structure. These porous aggregates further collided with each other to form increasingly more-porous structures. An analysis was performed to understand the importance of aggregate fractal structure and its effective density on the settling velocity. The size-density fractal dimension of the asphaltene aggregates was estimated to be in the range of $D_3 = 1.3-2.0$. These relatively low fractal dimensions suggest that the asphaltene aggregates are highly porous and very tenuous.

Introduction

Oil and gas have powered the world economy for the past century and will likely continue for at least the coming century. With the rapid depletion of conventional oil reservoirs, increased oil production from technologically challenging sources, such as heavy oil and the oil sands, has become the norm. In the case of the Canadian oil sands, the asphaltene content of the oil (bitumen) is high (∼16%−20%).[1] Asphaltenes are known to stabilize water-in-oil emulsions that are produced during bitumen froth production.[2] A recently commercialized technology of bitumen froth treatment relies on addition of a paraffinic solvent above the inception point of asphaltene precipitation.[3] The precipitated asphaltenes act as a flocculent to the emulsified water droplets and fine solids in the diluted froth. Clusters of precipitated asphaltenes, water droplets, and solids are formed, enabling their removal using gravity settling.[4,5] Thus, the properties of the flocs, especially their size, density and structure, which affect the settling rate, are of great importance for the process equipment design.

Aggregate size and density (or porosity) are the most important factors that influence the efficiency of aggregate removal from suspensions. It is well-known that aggregate size and density (or porosity) are often mutually dependent and can be expressed by some empirical relationships, such as a power-law-type relation.[6−9] In addition, shape or structure also affects the behavior of aggregated particles, particularly with regard to settling rates[6,7] and collision efficiency.[8,9] Solids removal efficiency by sedimentation or filtration is dependent on the structure of the aggregates, because this determines the relationship between aggregate size and density. Moreover, changes in aggregate structure within a suspension affect macroscopic properties, such as viscosity[10] and density.[11] The porosity of the aggregates also determines the quality of the aggregate compactness.[12]

Altering the mass, surface area, and number concentration of particles can substantially affect their removal by gravity sedimentation in a settling vessel. Informa-

* Author to whom correspondence should be addressed. Tel: 780-492-4673. Fax: 780-492-2881. E-mail: jacob.masliyah@ualberta.ca.
[†] University of Alberta.
[‡] CANMET.

(1) Strausz, O. P. *AOSTRA Technical Handbook of Oil Sands, Bitumen and Heavy Oils*; Hepler, L. G., His, C., Eds.; AOSTRA Technical Publications Series 6; AOSTRA: Edmonton, Alberta, Canada, 1989.
(2) Yarranton, H. W. Ph.D. Thesis, University of Alberta, Canada, 1997; pp 02, 20−21.
(3) Firmin, K. *Muskeg River Mine Froth Treatment Process*. Shell Canada, CIM Meeting, Edmonton, 2000.
(4) Long, Y.; Dabros, T.; Hamza, H. *Fuel* **2002**, *81*, 1945.
(5) Long, Y.; Dabros, T.; Hamza, H. *Fuel* **2004**, *83*, 823.
(6) Namer, J.; Ganczarczyk, J. J. *Water Pollut. Res. J. Can.* **1994**, *29* (4), 441−455.
(7) Johnson, C. P.; Li, X.; Logan, B. E. *Environ. Sci. Technol*. **1996**, *30*, 1911−1918.
(8) Jiang, Q.; Logan, B. E. *Environ. Sci. Technol*. **1991**, *25* (12), 2031−2037.
(9) Wiesener, M. R. *Water Res.* **1992**, *26*, 379−387.
(10) Gillespie, T. *J. Colloid Interface Sci*. **1983**, *94* (1), 166−173.
(11) Spicer, P. T.; Keller, W.; Pratsinis, S. E. *J. Colloid Interface Sci*. **1996**, *184*, 112−122.

10.1021/ef0496707 CCC: $30.25
Published on Web 04/23/2005

tion pertaining to the settling velocity of an individual aggregate is important, because it is possible to correlate the velocity of a cluster−cluster aggregate to the velocity of a primary cluster.[13] Aiba et al.[14] and Bradley and Krone[15] indicated that the average settling velocity of activated sludge suspended solids could be empirically expressed as a linear function of the settling velocity of individual particles. The coefficient of this function might be either a constant or a variable, which is dependent on the concentration of the solids.

Many studies have shown that the irregular aggregate shapes can be described in terms of fractal geometry concepts.[8,9,16,17] A complete characterization of a particle suspension should include a description of the fractal dimension of the aggregates.[8,16] Fractal geometry concept is useful in describing the rugged surface of large, irregular, porous aggregates that are not well-defined by Euclidean geometry. In this concept, area and volume are not generally calculated by raising the characteristic length of an object to an integer power. Heterogeneously (nonuniformly) packed objects with irregular boundaries can be defined by nonlinear relationships where the properties of the object scale with a characteristic length dimension raised to a power called the fractal dimension.[9,17] For example, the aggregate porosity (and the effective density) and aggregate size can be expressed by the following power-law relationships:

$$1 - \epsilon \propto l_a^{D-3} \tag{1}$$

$$\rho_{eff} = \rho_a - \rho_l = (1 - \epsilon)(\rho_p - \rho_l) \propto l_a^{D-3} \tag{2}$$

where ϵ is the aggregate porosity, the quantity $1 - \epsilon$ is the solid volume fraction in an aggregate, l_a is the characteristic size of the aggregate (e.g., the longest dimension is used for present study), ρ_{eff} is the aggregate effective density, ρ_a is the aggregate density (i.e., including the space between particles of an aggregate to determine aggregate encased volume), ρ_l is the density of the liquid, ρ_p is the density of the primary particles used to build the aggregate, and D is the three-dimensional fractal dimension for a self-similar structure. In eqs 1 and 2, the number 3 represents the Euclidean dimension for the three-dimensional space. Because the fractal dimension is usually less than the Euclidean dimension, eqs 1 and 2 indicate that the aggregate porosity increases and the effective density decreases as the aggregate size increases.[18]

The basic understanding of the structure and property of fractal aggregates is derived using the computer simulations.[19] Such models have been developed by many investigators (for example, Vold,[20] Lagvankar and Gemmell,[21] Meakin,[22] and Mountain et al.[23]). These studies have shown that the fractal dimension is dependent on the conditions of aggregate formation and that D may range from <1.7 to 3.0.[24] On the other hand, several experimental studies on the floc/aggregate porosity or density−size relationship have been performed by many investigators for flocs formed with different materials under various conditions. These studies have shown that the power law for floc porosity (or effective density) is valid at least over a limited range of floc sizes. In these experimental studies, various methods had been used to measure the floc density (e.g., the equivalent density method;[21,25] isopycnic centrifugation;[26] interference microscopy;[27] the Oden balance method and the photoextinction method;[28] and the free-settling test.[13,18,29,30] Among these methods, the free-settling test is the most widely used method in the literature, because of its simplicity and low cost.[31]

The information obtained in a free-settling test is the equivalent diameter and the terminal settling velocity of a single aggregate. Assuming that the aggregate moves steadily in the medium, a force balance is used to estimate the aggregate density (and also aggregate porosity). Based on the constructed aggregate "size−density" relationship, Li and Ganczarczyk[32] and Jiang and Logan[8] proposed that an aggregate is a highly porous fractal-like object that is comprised of many primary particles. The fractal dimension is a quantitative measure of how the primary particles occupy the aggregate interior space. In addition to the aggregate diameter and terminal velocity data, information about several parameters is required in the force balance equation, such as the drag coefficient,[18] the primary particle density,[33] and the correction factor for advection flow.[34]

So far, very few studies have been concerned with the physical aspects of asphaltenes flocculation, and little is known regarding the morphological characteristics of asphaltene flocs and the relation between their structure and settling properties. To gain knowledge on the physical and morphological aspects of the flocculation process of asphaltenes, this paper presents an experimental study using microscopic and optical monitoring techniques to study the structure of the asphaltene aggregates and their settling rate. For efficient removal of asphaltene aggregates from a suspension, it is important to understand the settling behavior of the

(12) Pierre, A. C.; Ma, K.; Barker, C. *J. Mater. Sci*. **1995**, *30* (8), 2176−2181.
(13) Li, D. H.; Ganczarczyk, J. *Water Res*. **1987**, *25* (9), 1137−1143.
(14) Aiba, S.; Humphrey, A. E.; Millis, N. F. *Biochemical Engineering*; University of Tokyo Press: Tokyo, 1965.
(15) Bradley, R. A.; Krone, R. B. *J. Sanit. Eng. Div., Am. Soc. Civ. Eng*. **1971**, *97*, 59−79.
(16) Gorczyca, B.; Ganczarczyk, J. *Environ. Technol.* **1996**, *17*, 1361−1369.
(17) Logan, B. E. *Environmental Transport Processes*; Wiley: New York, 1999; pp 443−453.
(18) Huang, H. *Clays Clay Miner.* **1993**, *41* (3), 373−379.
(19) Meakin, P. *Adv. Colloid Interface Sci*. **1988**, *28* (4), 249−331.
(20) Vold, M. J. *J. Colloid Sci*. **1963**, *18*, 684−695.
(21) Lagvankar, A. L.; Gemmell, R. S. *J.−Am. Water Works Assoc.* **1968**, *60*, 1040−1046.
(22) Meakin, P. *Phys. Rev. A: Gen. Phys.* **1984**, *29*, 997−999.
(23) Mountain, R. D.; Mulholland, G. W.; Baum, H. *J. Colloid Interface Sci*. **1986**, *114*, 67−81.
(24) Rogak, S. N.; Flagan, R. C. *J. Colloid Interface Sci*. **1990**, *134* (1), 206−218.
(25) Gibbs, R. J. *J. Geophys. Res*. **1985a**, *90*, 3249−3251.
(26) Dammel, E. E.; Schroeder, E. D. *Water Res.* **1991**, *25*, 841−846.
(27) Andreadakis, A. D. *Water Res.* **1993**, *27*, 1707−1714.
(28) Matsumoto, K.; Mori, Y. *J. Chem. Eng., Jpn*. **1975**, *8* (2), 143−147.
(29) Tambo, N.; Watanabe, Y. *Water Res*. **1979**, *13*, 409−419.
(30) Lee, D. J.; Hsu, Y. H. *Environ. Sci. Technol.* **1994**, *28*, 1444−1449.
(31) Lee, D. J.; Chen, G. W.; Liao, Y. C.; Hsieh, C. C. *Water Res*. **1996**, *30*, 541−550.
(32) Li, D. H.; Ganczarczyk, J. *Environ. Sci. Technol.* **1989**, *23*, 1385−1389.
(33) Lee, D. J. *J. Chem. Technol. Biotechnol.* **1994**, *61*, 139−144.
(34) Logan, B. E.; Hunt, J. R. *Limnol. Oceanogr.* **1987**, *32* (5), 1034−1048.

fractal aggregates. This study involves performing the measurements of settling velocities for several aggregates within a glass-settling column and investigating the relationship among the porosity, permeability, and settling velocity of fractal aggregates. An aggregate-settling model that considers the effect of creeping flow through the aggregate on its settling velocity is used in the aggregate porosity calculations. The three-dimensional (3-D) fractal dimensions of the aggregates are then determined from the slopes of the size−effective-density regression lines.

Governing Equations for Aggregate-Settling Model. In this article, a free-settling test is defined as settling through an unbounded fluid where the size and settling velocity of the aggregates are measured in a quiescent glass column. Assuming that settling of each individual aggregate satisfies Stokes' law, the porosity (ϵ) of an aggregate is determined from

$$1 - \epsilon = \frac{18\mu U}{g(\rho_p - \rho_l)d_a} \tag{3}$$

where U is the measured aggregate settling velocity, d_a is the aggregate diameter, μ is the dynamic viscosity of liquid medium, g is the gravity acceleration, ρ_l is the density of liquid medium, and ρ_p is the density of primary particles in the aggregate.

Equation 3 is questionable, because Stokes' law is only valid for an impermeable, spherical particle. Because an aggregate has highly porous structure, the ambient fluid penetrates the aggregate and the settling velocity of the aggregate is, therefore, higher than that of an impermeable particle with the same size and the same effective density as the aggregate.[35−37] Considering these effects, in general, the force balance for an aggregate moving steadily in an infinite medium can be described by[18,35−38]

$$U = \left[\frac{4}{3}\frac{g(1-\epsilon)}{\Omega C_D}\frac{\rho_p - \rho_l}{\rho_l}d_a\right]^{1/2} \tag{4}$$

The porosity of the aggregate then can be obtained as

$$\frac{\rho_a - \rho_l}{\rho_p - \rho_l} = \frac{\rho_{eff}}{\rho_p - \rho_l} = 1 - \epsilon = \frac{3\rho_l \Omega C_D}{4g(\rho_p - \rho_l)d_a}U^2 \tag{5}$$

where C_D is the drag coefficient, ρ_a is the aggregate density, and Ω is the ratio of the resistance experienced by an aggregate to that of an equivalent solid sphere. Except for the aggregate diameter and terminal velocity data, which are available from experimental measurements, four unknowns are present in eq 5: ρ_p, Ω, C_D, and ϵ/ρ_{eff}. To estimate the aggregate porosity or effective density, three values (ρ_p, Ω, and C_D) are required.

Determination of Model Parameters. As in most previous studies, the present study also assumes that ρ_p is equal to ρ_s, which represents the dried solid density.[18,29]

Making use of the Brinkman permeability model, which is applicable for highly porous aggregates (up to 99% porosity), the drag force factor or permeability correction factor (Ω) is given by

$$\Omega = \frac{2\beta^2[1 - (\tanh\beta)/\beta]}{2\beta^2 + 3[1 - (\tanh\beta)/\beta]} \tag{6}$$

where

$$\beta = \frac{d_a}{2\sqrt{k}} \tag{7}$$

and the permeability k is defined by

$$k = \frac{d_p^2}{72}\left[3 + \frac{4}{1-\epsilon} - 3\sqrt{\frac{8}{1-\epsilon} - 3}\right] \tag{8}$$

Because the experimentally observed Reynolds number ($Re = Ud_a\rho_l/\mu$) is in the range of 0.006−0.136 in the present study, the drag coefficient is given by

$$C_D = \frac{24}{Re} \tag{9}$$

Equations 6−9 provide closure to the present aggregate-settling model. They were substituted into eq 5 and, assuming d_p is known, the equation contains only one unknown: the aggregate porosity or density.

Experimental Method

Preparation of Asphaltene Aggregates. The vacuum-distillation-tower-feed Athabasca bitumen (that has been treated to remove most of the solids and water and is obtained from Syncrude Canada, Ltd.) is used in this study to derive solid asphaltenes from bitumen using a standard procedure, which is described elaborately in a previous paper.[39] The asphaltene aggregates then are produced in a bench-scale continuous stirred tank reactor with a volume of 1.0 L at different fluid shear rates (36, 75, and 160 rpm). The impeller is a standard 45°-angle four-blade pitch turbine, and the suspension is mixed by the impeller with the presence of a baffle. The center of the impeller is positioned one-third of the tank height from the bottom and rotated clockwise to provide a downward pumping direction. This type of axial flow creates good top-to-bottom motion in the tank, which results in good mixing. It is possible to vary the speed and time of both the rapid mix and slow stirring phases, using a variable-speed motor controller (model RZR 50, Caframo, Canada).

For the first set of flocculation experiments, samples of dried asphaltenes were dissolved in toluene to give a concentration of 375 mg/L. The asphaltenes in toluene solution were then added to pure *n*-heptane in a continuous stirred tank reactor to give an asphaltene concentration of 62.5 mg/L in the toluene−heptane solvent mixture. Formed asphaltenes precipitate in the solvent mixture, which was first mixed at 660 rpm for 15 s to homogenize the mixture. The solvent composition (i.e., the final toluene:heptane volume ratio in the solution) was fixed at 1:5. The impeller was then set to the desired speed. Two different stirring speeds (36 and 75 rpm) were used in two separate experiments.

In the second set of flocculation experiments, 960 mg of bitumen was dissolved in 160 mL of toluene and the solution was added to 800 mL of *n*-heptane in the stirred tank to give a bitumen concentration of 1000 mg/L in the toluene−heptane

(35) Neale, G.; Epstein, N.; Nader, W. *Chem. Eng. Sci*. **1973**, *28*, 1865−1874.
(36) Matsumoto, K.; Suganuma, A. *Chem. Eng. Sci*. **1977**, *32*, 445−447.
(37) Masliyah, J. H.; Polikar, M. *Can. J. Chem. Eng*. **1980**, *58*, 299−302.
(38) Li, D. H.; Ganczarczyk, J. *Water Environ. Res.* **1992**, *64*, 236−240.
(39) Rahmani, N. H. G.; Dabros, T.; Masliyah, J. H. *Ind. Eng. Chem. Res*. **2005**, *44*, 75−84.

solvent mixture. The precipitated asphaltenes in the solvent mixture were instantly mixed at 660 rpm for 15 s, to homogenize the mixture. It has been reported that the heptane-insoluble asphaltenes content of Athabasca bitumen is ~16 wt %.[40] Therefore, it gives an equivalent asphaltenes concentration of ~160 mg/L in the bitumen concentration of 1000 mg/L. The ratio of toluene to *n*-heptane was kept fixed at 1:5, and the stirring speed varied to be 75 and 160 rpm during ramped-shear flocculation. For ramped-shear experiments, the aggregates were first allowed to grow at 75 rpm and a steady-state aggregate size was formed. After 60 min, the stirring speed then was instantly increased to 160 rpm, a new steady-state aggregate size was reached, and the suspension was mixed at this speed for 60 min. The samples of asphaltene aggregates were collected at the corresponding steady states for the free-settling tests.

Stirred-Tank Flow-Field Characterization. The parameter most frequently used to express energy input in a stirred tank is the volume-averaged shear rate (G_{avg}), which is given by[41]

$$G_{avg} = \sqrt{\frac{P_l}{\mu V_t}} = \sqrt{\frac{\xi}{\nu}} \tag{10}$$

where P_l is the energy dissipated into the liquid (in watts), μ is the dynamic viscosity of the suspending liquid (given in units of Pa·s), V_t is the suspending liquid volume in the stirred tank where the energy is applied (given in units of m^3), ξ is the energy dissipation rate per unit mass ($\xi = P/M$; given in units of m^2/s^3), M is the mass of liquid (in kilograms), and ν is the kinematic viscosity of the liquid ($\nu = \mu/\rho_l$, where ρ_l is the density of the liquid (given in units of kg/m^3); ν is given in units of m^2/s). According to Godfrey et al.[42] and Clark and Flora,[43] the rate of dissipation of energy is given by

$$\xi = \frac{P_0 N_{rps}^3 D_{imp}^5}{V_t} \tag{11}$$

where P_0 is the impeller power number (dimensionless), N_{rps} is the impeller rotational rate (given in units of rev/s), and D_{imp} is the impeller diameter (in meters). The impeller Reynolds number (Re_{imp}) varied from 2×10^3 to 35×10^3 in the present work. The volume-averaged shear rate G_{avg} is calculated using a power number, $P_0 = 1.2$, for the applied 45°-angle four-blade pitch turbine and turbulent flow ($Re_{imp} > 10^3$) (see Figure 3.16 on p 63 in the book of Oldshue[44]) and combining eqs 10 and 11. The flow conditions within a stirred tank are nonhomogeneous;[45] thus, the G_{avg} value in eq 10 does not characterize the local velocity gradient (i.e., in the impeller or bulk zones of the mixing tank) or the velocity fluctuations experienced in the stirred tank.[46] It is used solely as a basis for comparison of the various shear rates effect on the aggregation process. Table 1 shows the experimental values of Re_{imp} and G_{avg}, as applied in this work.

Settling Apparatus and Experiment. The asphaltene aggregates that were produced in a bench-scale continuous stirred tank reactor at different fluid shear rates (36, 75, and 160 rpm) were used in the free-settling tests to determine the settling velocities. The experimental apparatus for the settling of asphaltene aggregates consists of a Pyrex glass column (see Figure 1). The column is 350 mm in height, and it is sufficiently long to ensure that the terminal settling velocity is reached. The column width is 30 mm, and the ratio of column width to the maximum aggregate length is ~150 (= 30000 μm/200 μm). With such a large value, one can neglect the wall effect on aggregate settling. After the average aggregate diameter reached a steady-state size (which is known from the previously performed growth kinetics experiments using Photometric dispersion analyzer),[39] samples were withdrawn from the stirred tank at intervals of 15 min. A small amount (~3 mL) of suspension containing aggregates is gently transferred into the top of the settling column, using a rubber dropper bulb with a 10-mL pipet tip cut midway to minimize breakup of the aggregates. The column was filled with a toluene and heptane solvent mixture at a volume ratio of 1:5, which is the same as the solvent ratio in the stirred tank. Images of the asphaltene aggregates, while passing through the observation region in the glass-settling column, were obtained using a microscope objective (Carl Zeiss Canada, Ltd.), coupled with a charge-coupled device (CCD) camera and a video recorder. A cold fiber-optic light was placed on the same side of the column as the camera, to provide reflected lighting from the white background on the other side of the column, and the camera produced clear and sharp pictures.

Table 1. Range of Reynolds Numbers and Average Shear Rates for the Present Study

impeller rotational speed, N_{rps} (rev/s)	Reynolds number of impeller, Re_{imp}[a]	average shear rate, G_{avg} (s^{-1})[b]
36/60	1.9×10^3	10
75/60	4.0×10^3	28
160/60	8.6×10^3	87
660/60	35.4×10^3	730

[a] $Re_{imp} = N_{rps} D_{imp}^2 \rho/\mu$. [b] $G_{avg} = [(P_0 N_{rps}^3 D_{imp}^5/V_t)(\mu/\rho)]^{1/2}$.

Experimental Analysis. The video recordings were obtained on a VHS high-grade videotape. The Snappy Video Snapshot program, which was installed under Windows XP, was used to grab and digitize the chosen frames of the recordings. Sigma Scan Pro automated image analysis software was used to determine the shape, size, and settling velocity of the aggregates from the captured images. To determine the aforementioned parameters, a sequence of few frames was grabbed and digitized at various observation times. An identical procedure was always applied in image analysis of the grabbed frames. The background light intensity varied continuously, depending on the number and size of the aggregates passing through the observation region; thus, the automatic gray-scale filtering could not be used. Therefore, the objects on a frame were filled using manual tracing of the boundaries for geometric characterization. Several parameters such as area, projected area diameter, major axis or longest dimension, and shape factor were determined for each aggregate. The projected area diameter of an aggregate (d_a) is defined as

$$d_a = \sqrt{\frac{4 \times \text{Area}}{\pi}} \tag{12}$$

This is the diameter of a circular object that has the same projected or cross-sectional area as the irregular object being measured. The major axis, as provided by the image analysis software, is used to characterize the aggregate structure, in terms of fractal dimension. The geometric characteristics and distance between the aggregates at two different captured photographs were measured using an image analysis system. To interpret the image size correctly, a graduated microscale was photographed to determine the number of pixels corresponding to a given standard length for each set of experiments.

(40) Rahmani, N. H. G. Ph.D. Thesis, University of Alberta, Canada, 2004, p 14.
(41) Camp, T. R.; Stein, P. C. *J. Boston Soc. Civ. Eng.* **1943**, *30* (4), 219.
(42) Godfrey, J. C.; Obi, F. I. N.; Reeve, R. N. *Chem. Eng. Prog.* **1989**, *85* (12), 61.
(43) Clark, M. M.; Flora, J. R. V. *J. Colloid Interface Sci.* **1991**, *147* (2), 407.
(44) Oldshue, J. Y. *Fluid Mixing Technology*; McGraw−Hill: New York, 1983.
(45) Cutter, L. A. *AIChE J.* **1966**, *12*, 35.
(46) Cleasby, J. L. *J. Environ. Eng.* **1984**, *110* (5), 875.

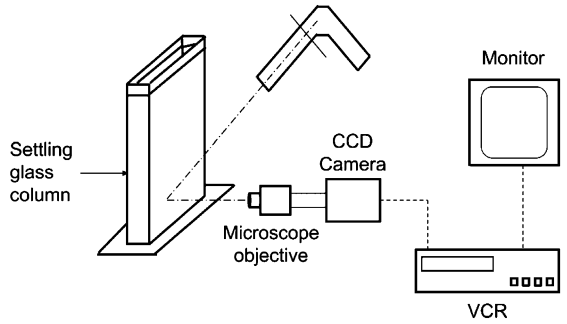

Figure 1. Experimental arrangement for aggregate settling velocity measurement.

To determine the aggregate settling velocity, frames i and $i + 1$ were captured and processed using the image analysis software. Frame i is captured when the aggregate enters the viewing area, and frame $i + 1$ is captured when the aggregate is about to leave the viewing area. As a result, two positions (i.e., the initial and final positions) of an aggregate within a known time interval, Δt (number of fields advanced at the normal playback speed of a video cassette, multiplied by $^1/_{30}$ s) were obtained on frames i and $i + 1$, and the distance between two positions of every aggregate was measured. The settling velocity (U) of an aggregate was calculated as

$$U = \frac{\sqrt{(x_2 - x_1)^2 + (y_2 - y_1)^2}}{\Delta t} \cong \frac{\sqrt{(y_2 - y_1)^2}}{\Delta t} \qquad (13)$$

where (x_2,y_2) and (x_1,y_1) are coordinates of the center of an aggregate on frames $i + 1$ and i, respectively, and Δt is the time interval between the frames. It was observed from the experiments that the horizontal movement of the aggregates (i.e., $x_2 - x_1$) was negligible, compared to the vertical movement (i.e., $y_2 - y_1$). Knowing the magnification, traveling distance, and time between two positions for a given aggregate, the terminal settling velocity was calculated. The distance $y_2 - y_1$ in the captured images was ~2.5 mm (= 2500 μm), and the largest d_a observed in experiments was ~200 μm. Hence, the error associated with the settling velocity calculation should be ~5%−10%. Second, because the experimentally observed settling velocities were very low ($Re = 0.006-0.136$), rotation of the aggregates was not observed.

Results and Discussion

Settling Velocities in Toluene−Heptane Solvent Mixtures. During this set of tests, the settling velocity and size of a large number of asphaltene aggregates are measured. The area-equivalent diameter of the aggregates are in the range of 20−200 μm, and the settling velocities are in the range of ~100−600 μm/s, corresponding to the Reynolds number ($Re = Ud_a\rho_l/\mu$, where $\rho_l = 714.5$ kg/m^3 and $\mu = 0.45$ mPa·s, which corresponds to a toluene and heptane solvent mixture of 1:5 volume ratio at a temperature of 20 °C) in the range of $Re = 0.006-0.136$. The settling velocities are shown in Figure 2a and b, as function of the projected area diameter of the aggregates. Other size characteristics, such as volume-equivalent diameter or surface-area-equivalent diameter, could not be derived from image analysis measurements and are not considered.

Figure 2a presents the relationship between the projected area diameter and the terminal settling velocity of asphaltene aggregates that were formed at two different shear rates (i.e., 36 and 75 rpm). The aggregates are produced from extracted asphaltenes. The

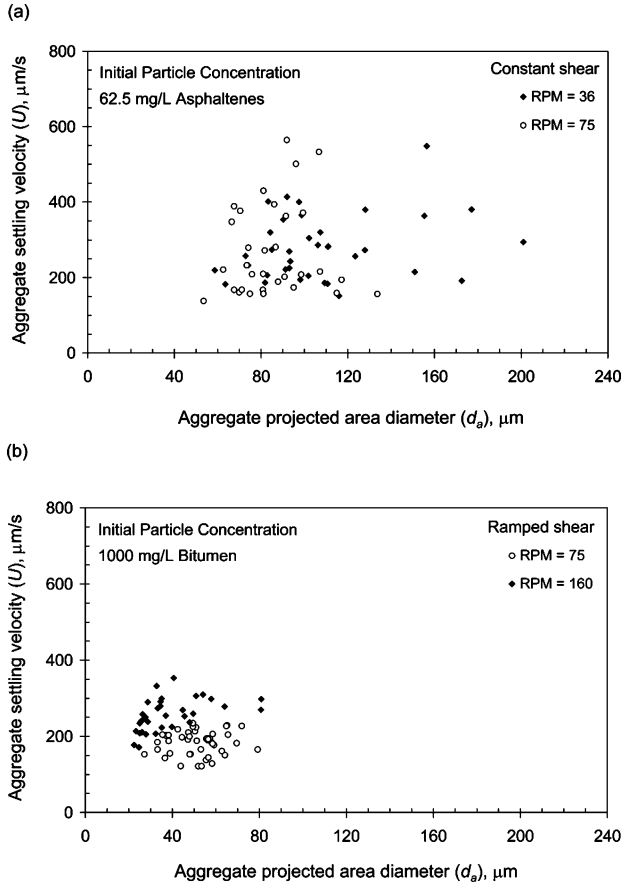

Figure 2. Aggregate settling velocity as a function of the projected area diameter at different shear rates for toluene-to-heptane solvent ratio (T:H) of 1:5.

open circles are the observed settling velocities at 36 rpm, and the solid squares are the data points at 75 rpm. With the projected area diameter as the size criterion, the data are quite scattered. No significant difference is observed in the settling velocities for aggregates obtained at two different shear rates. If solid (i.e., nonporous) spherical particles of similar diameters are considered, then the Stokes velocities would be at least an order of magnitude higher than the settling velocities observed in the tests. This would indicate that the asphaltene aggregates are highly porous. A larger variance of experimental data, especially for larger aggregates, was also observed by Ganczarczyk and coworkers.[6,16] This could be caused either by the limitations of the experimental method used or by the real shape distribution of asphaltene aggregates within the same characteristic length.

Figure 2b shows the settling velocities of asphaltene aggregates, produced from bitumen during ramped shear, initially at 75 rpm and then at 160 rpm. The solid squares are the observed settling velocities at 75 rpm, and the open triangles are the data points at 160 rpm. Note that, for the same projected area diameter of the aggregates (d_a), the observed settling velocities at 160 rpm are significantly higher than those observed at 75 rpm. It implies that higher shear produces more-compact and denser aggregates. This is in agreement with the concept of mechanical syneresis described by Yusa,[47] because shrinkage and densification of loose and

(47) Yusa, M. *Int. J. Miner. Process.* **1977**, *4*, 293−305.

bulky aggregates occur due to the shear force that is being applied locally, unevenly, and fluctuating over the surface of the aggregates. This is also consistent with experimental results of Klimpel and Hogg[48] for quartz flocs and Huang[18] for drilling mud flocs.

It is observed from the experimental results that, in some cases, the aggregate-settling velocities did not increase as the aggregate size is increased. This can probably be explained by the irregular shapes of the aggregates, which have significant effects on the settling velocities of nonspherical particles. Although the effect of fluid drag force on the settling velocity of a particle is dependent on the nonsphericity of the particle, it could be up to twice as great for nonspherical particles than for spherical particles.[49,50] Furthermore, aggregates with the same volume but different shape can settle at different rates. According to Lerman,[49] the expected settling rates, from fastest to slowest, are for sphere, cylinder, needle, and disk, respectively. Thus, a disk-shaped or cylindrical floc may settle more slowly than a spherical floc with the same volume, even though the longest dimension of the disk or cylinder may be larger than that of the spherical floc. Moreover, floc-settling velocity is also affected by the settling orientations of the flocs, because the drag force is dependent on the area facing the settling direction, whereas the effective gravitational forces are dependent on the volume. This influence may exist in asphaltene aggregate-settling tests that usually occur in a creeping-flow region, because nonspherical particles can settle at many possible orientations in this region.[51] However, in this analysis, the influence of the possible flow through the aggregate, which also affects the drag force, has been taken into consideration by solving eqs 6−9.

Porosity and Effective Density of Asphaltene Aggregates. The aggregate porosities are calculated according to eq 5 and are plotted against the projected area diameter, as shown in Figure 3a. In the calculation of aggregate porosities, the values used for the different variables are $\rho_p = 1200$ kg/m^3 (assuming solid asphaltene as the primary particle), $\rho_l = 714.5$ kg/m^3, and $\mu = 0.45$ mPa s (which corresponds to a toluene and heptane solvent mixture of 1:5 volume ratio at a temperature of 20 °C). A range of d_p values —equal to 0.1, 1.0, and 5.0 μm—is used to calculate the aggregate porosities, because it was not possible to determine the primary particle size, because of experimental constraints. When the porosity of the aggregates is known, the effective density can be estimated using eq 5. The obtained porosities are used to determine aggregate effective densities and are shown in Figure 3b.

The observed relationship between the porosity of the aggregates and their projected area diameter confirms the general increase of aggregate porosity with increasing size, with a rapid increase in porosity in the <50 μm size range of the aggregates, i.e., the porosity ranges from ~0.35−0.85 for d_a values, increasing from 25 μm to 50 μm (see Figure 3a). Higher porosity of the aggregates with an increasing characteristic length indicates that the structure of the aggregates possesses a space-filling capacity in which the nonsolid portion is relatively high, and the aggregate projected area is, therefore, not completely filled.[52] This phenomenon is also confirmed from the smaller values of the experimentally observed 3-D fractal dimensions ($D < 2$). (See Figure 7, presented later in this work.)

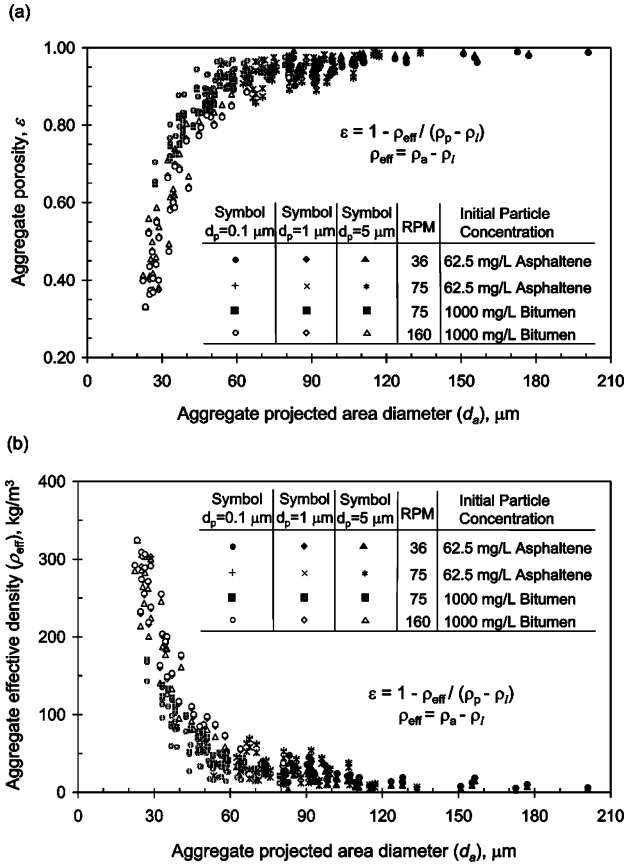

Figure 3. Scattered plot of porosity and effective density of asphaltene aggregates versus their projected area diameter for different experimental conditions.

Figure 3a shows that the asphaltene particle concentration at which the aggregates are formed has no distinguishable effect on aggregate porosity. This is inferred, because the porosities calculated at 75 rpm from experimental observations (shown by plus symbols and shaded plus symbols for $d_p = 0.1$ μm; cross symbols and shaded cross symbols for $d_p = 1.0$ μm; star symbols and shaded star symbols for $d_p = 5.0$ μm) represent aggregates formed at two different particle concentrations. The aggregates formed with bitumen had a higher particle concentration (bitumen concentration of 1000 mg/L, which is roughly equivalent to asphaltene particle concentration, ≅160 mg/L) than aggregates formed with extracted asphaltenes (asphaltene particle concentration of 62.5 mg/L). However, no difference in aggregate porosities was observed. Although some scattering exists, the data suggest that, for the same size, the aggregates formed at different particle concentrations but at the same shear rate may have the same porosity. Moreover, the shift to lower porosities (see Figure 3a), i.e., higher effective densities (see Figure 3b), for smaller

(48) Klimpel, R. C.; Hogg, R. *J. Colloid Interface Sci.* **1986**, *113* (1), 121−131.
(49) Lerman, A. *Geochemical Processes: Water and Sediment Environment*; Wiley: New York, 1979.
(50) Ozturgut, E.; Lavalle, J. W. *Environ. Sci. Technol.* **1984**, *18*, 947−952.
(51) Allen, T. *Particle Size Measurement, Vol. 1*; Chapman and Hall: London, 1997.
(52) Namer, J.; Ganczarczyk, J. J. *Water Res.* **1993**, *27* (8), 1285−1294.

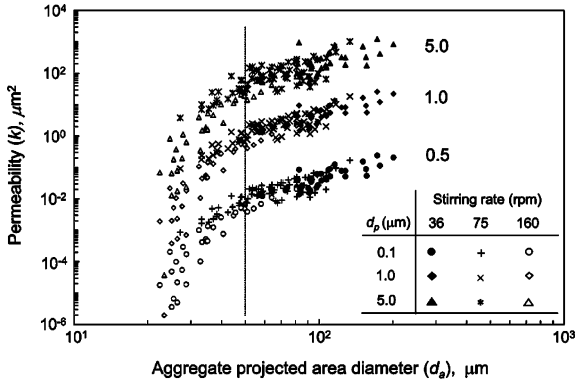

Figure 4. Aggregate permeability calculated from Brinkman model versus aggregate projected area diameter (d_a) at different shear rates and primary particle sizes (d_p).

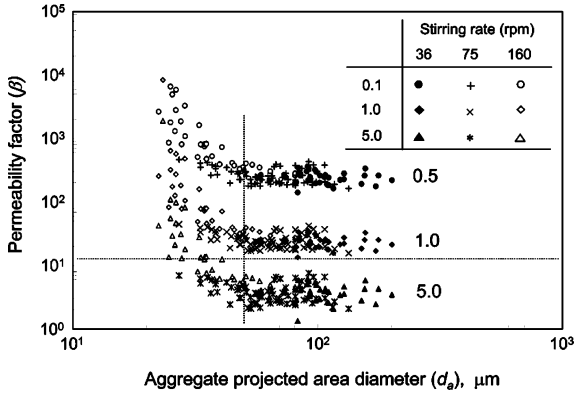

Figure 5. Permeability factor β, a dimensionless group, is plotted against aggregate projected area diameter (d_a). Brinkman model is used and a critical β value of 10.9 is shown by the horizontal dotted line.

aggregates is mostly observed for aggregates formed at higher shear rates (estimated from the dominance of open symbols in Figure 3) and is caused by their more-compact structures. Also, the aggregate porosity was determined to be fairly independent of the d_p values used (this was understood from the overlapping of the symbols used for three different d_p values).

Permeability of Asphaltene Aggregates. The permeability of asphaltene aggregates was calculated using the Brinkman model (eq 8) for three different d_p values (0.1, 1.0, and 5.0 μm) and is shown in Figure 4. For the smaller aggregate size, the permeability k rapidly increases as the aggregate diameter increases. Then, at comparatively larger aggregate sizes, a smaller increase in the k values is observed. Within the aggregate diameter range studied, k varies over a range of $10^{-17}-10^{-9}$ m^2. Based on the same parameters (ρ_p and d_p), a higher shear rate reduces the permeability k by compacting the aggregate and decreasing porosity (see Figure 4). Lee et al.[31] has reported a comparison of six different permeability models. They found that, for a specific aggregate size, the k values calculated from various models usually vary within a range of 2−3 orders of magnitude. The permeabilities from the Happel and Brinkman models are lower than the estimations by the Carman−Kozeny model for a spherical primary particle shape.

With the calculated aggregate permeability, the β values are shown in Figure 5. Although greatly scattered, when the aggregate size is smaller than ~50 μm,

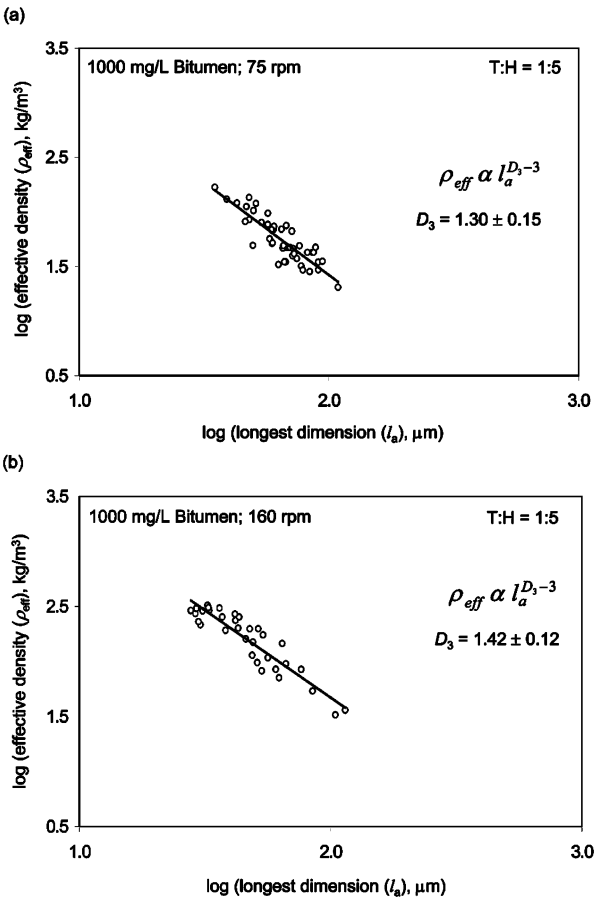

Figure 6. Relationship between the log of aggregate effective density (ρ_{eff}) and longest dimension (l_a) with the plot of nonlinear regression model to determine three-dimensional fractal dimensions (D_3) of aggregates formed with bitumen. (In Figure 6(a), stirring rate = 75 rpm; and in 6(b), stirring rate = 160 rpm).

the β values show a clear ascending trend with decreasing aggregate size. Above this 50 μm size range threshold, the β values are observed to be almost constant with aggregate diameter. Because β is inversely proportional to k, based on the same parameters (ρ_p and d_p), the β value is larger at higher shear rates. Li and Ganczarczyk[38] defined a critical β value of 10.9, below which the aggregate can be viewed as a permeable aggregate. Because ρ_p is constant and d_p is the only variable parameter for calculations in present work, in Figure 5 with d_p = 5.0 μm, almost all the aggregates produced at different shear rates are permeable. In contrast, with d_p = 0.1 μm, all aggregates become impermeable and the aggregates produced with d_p = 1.0 μm fall close to the borderline range between permeable and impermeable. Based on this estimation, it can be inferred from Figure 5 that a larger aggregate is not always more permeable than a smaller aggregate.

It was not possible, with the present experimental arrangement, to determine an exact value for d_p; therefore, a range of d_p values was studied, to accommodate the real d_p value for the aggregates on somewhere of the parameter space studied. Hence, the possible error for aggregate permeability estimation will be as high as few orders of magnitude. Therefore, caution must be exercised with any conclusion drawn from the aggregate permeability information thus obtained.

Table 2. Three-Dimensional (3-D) Fractal Dimensions under Various Conditions for All Data

	Fractal Dimension, D_3 (± Standard Error)			
	Asphaltene Aggregates Formed with Asphaltene (62.5 mg/L)		Asphaltene Aggregates Formed with Bitumen (1000 mg/L)[a]	
model for dimensionless drag force factor (Ω)	36 rpm (G_{avg} = 10 s^{-1})	75 rpm (G_{avg} = 28 s^{-1})	75 rpm (G_{avg} = 28 s^{-1})	160 rpm (G_{avg} = 87 s^{-1})
impermeable (Ω = 1)	1.68 ± 0.20	1.59 ± 0.42	1.33 ± 0.15	1.44 ± 0.12
permeable (Brinkman model; Ω determined from eq 5.9)	1.87 ± 0.19	2.00 ± 0.38	1.30 ± 0.15	1.42 ± 0.12

[a] Equivalent asphaltene concentration ≅ 1000 × 0.16 = 160 mg/L

Using eq 6, the correction factor Ω can be calculated, and, as the aggregate permeability factor β, exceeds ~100, Ω approaches unity.[53] It indicates that the aggregate can be assumed to be an impermeable sphere. However, at smaller β values (less than ~50), the correction associated with the permeable structure of the aggregates is significant (i.e., the Ω value is less than unity). For example, Ω = 0.98 at β = 50, Ω = 0.42 at β = 2, and at the critical β value of 10.9, as defined by Li and Ganczarczyk,[38] Ω = 0.90. Hence, the Ω = 1 assumption for β values above the critical value produces an acceptable error (≤10%).

Fractal Dimensions (D_3) of Asphaltene Aggregates. The longest dimension (l_a) and the settling velocity (U) of the aggregate have been measured independently for each aggregate; therefore, these data have been used to estimate the aggregate effective density (ρ_{eff}), as a function of aggregate characteristic size (l_a) (see eq 2). Many researchers have investigated the relationship between effective density and a characteristic aggregate length, using various techniques, and observed a large variability in the dependency of ρ_{eff} on the aggregate length.[54] This has a major influence on predictions of aggregate settling velocity in practical situations. In the present study of asphaltene aggregates settling behavior, the difference in the slopes of Figure 6 can be explained by the evolution of the fractal nature of the aggregates under shear.

Three-dimensional fractal dimension, D_3 (also referenced as D), can be used to quantify the disorder aspect or the packing factor of an object. Its value varies from 1 to 3, where a value of 3 corresponds to a solid spherical structure. One distinct property of a fractal is power-law behavior. Hence, when an aggregate is fractal, it means that the effective density of the cluster varies with the diameter, according to the expression in eq 2. Figure 6 shows a log−log plot of the effective density versus the longest dimension for permeable asphaltene aggregates. The straight lines in Figure 6 are the least-squares fitted lines for data and, according to the relationship in eq 2, the slopes of these straight lines give a measure of the fractal dimension of the aggregates.[30] The standard error is applied in determining the slopes from the regression lines.

Figure 6a and 6b represent asphaltene aggregates formed with bitumen at 75 and 160 rpm, respectively. Based on the same aggregate diameter, at 160 rpm, the aggregate effective density is significantly higher (see Figure 6b) and the observed settling velocities are distinctly faster (see Figure 2b) than those observed at 75 rpm. This implies that asphaltene aggregates form more-compact structures at a higher shear. However, surprisingly, we did not observe a statistically significant difference in the 3-D fractal dimension between 75 rpm (1.30 ± 0.15) and 160 rpm (1.42 ± 0.12) (see Table 2). This might be due to scattering of experimental data points for the very narrow aggregate size range (20−90 μm) studied.

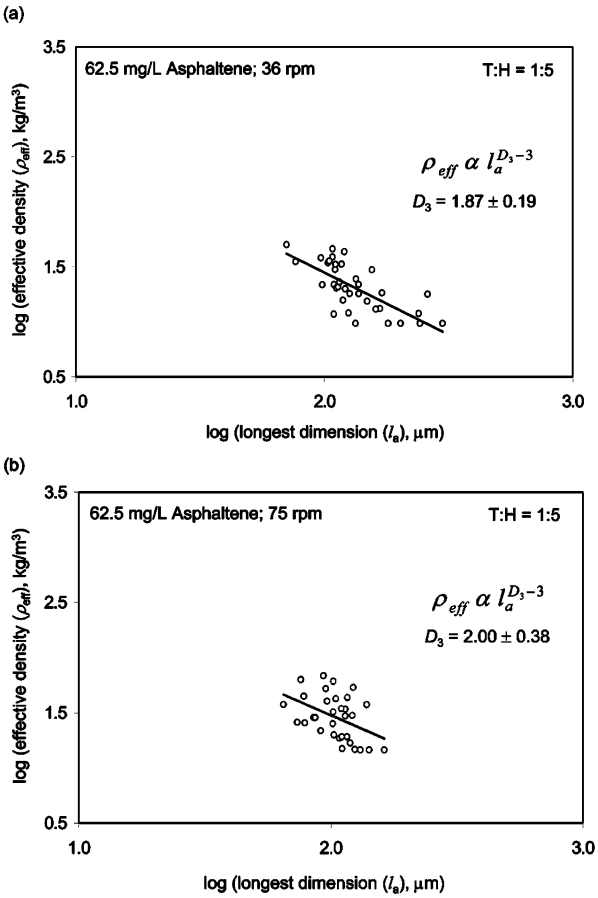

Figure 7. Relationship between the log of aggregate effective density (ρ_{eff}) and longest dimension (l_a) with the plot of nonlinear regression model to determine three-dimensional fractal dimensions (D_3) of aggregates formed with pure asphaltenes. (In Figure 7(a), stirring rate = 36 rpm; and in 7(b), stirring rate = 75 rpm).

Figures 7a and 7b represent asphaltene aggregates formed with extracted asphaltenes at 36 and 75 rpm, respectively, and no significant difference in the fractal dimension can be observed. However, when the permeable aggregate structures are considered at 75 rpm, the fractal dimension observed for asphaltene aggregates formed with extracted asphaltenes (2.00 ± 0.38) is appreciably higher than that with bitumen (1.30 ± 0.15). Because the solid concentration at which the

(53) Wu, R. M.; Lee, D. J. *Water Res.* **1998**, *32*, 760−768.
(54) Sternberg, R. W.; Berhane, I.; Ogston, A. S. *Mar. Geol.* **1999**, *154*, 43−53.

aggregates are formed has no distinguishable effect on aggregate porosity/density (see Figure 3), the significant difference in the aggregate structure might be happening because of the difference in aggregation mechanism in the presence of other compounds in bitumen (e.g., bitumen contains resins, aromatics, and saturates, along with asphaltenes).

Table 2 shows the calculated fractal dimensions under different conditions, assuming both permeable and impermeable aggregates. It can be observed from Table 2 that, when the asphaltene aggregates are formed with bitumen (shown on the right half of Table 2), the obtained fractal dimension is insensitive to the permeability model or the parameter set applied, because of the high β (or near unity Ω) values of comparatively smaller size aggregates. However, the obtained fractal dimension is significantly higher when the permeability of the aggregates is accounted for and when extracted asphaltenes are used for aggregate formation (shown on the left half of Table 2). It shows again that the effect of permeability on the settling velocity of an aggregate cannot be neglected at lower β values. Previously, the effect of permeability on the settling velocity of a porous sphere was theoretically discussed by Ooms et al.,[55] Sutherland et al.,[56] and Neale et al.,[35] and Matsumoto and Suganuma[36] experimentally showed that the effect of permeability on the settling velocity of a highly porous aggregate could not be neglected.

Because the correlations for the drag coefficient (C_D) and Ω values for a permeable sphere under creeping-flow conditions have a sound theoretical base, the free-settling test for smaller flocs provides a qualitatively valid aggregate density approximation. As a matter of fact, no direct evidence against the validity of the free-settling test on aggregates with a Reynolds number less than unity has been found.[31]

Conclusions

A remotely operated video system, comprised of a quiescent settling column, cold illuminating light, and frame grabber of video recording, has been used to collect time-lapsed sequences of settling aggregates. Image analysis of the video images collected on the computer provides independent estimates of particle size, shape, and settling velocity.

Suspended-aggregate sizes range from 20 μm (lower limit of detection) to 200 μm. Measurements of the aggregate settling velocity for the data set are in the range of 100−600 μm/s. Experimental data on the relationship between the terminal settling velocities of asphaltene aggregates and their projected area diameters demonstrated that the asphaltene aggregates are highly porous, and higher shear rate produces more-compact and denser aggregates. Apparently, the asphaltene particles form larger and "fluffy" aggregates at lower shear rates (e.g., 36 rpm).

Although many researchers have attempted to develop equations to calculate drag coefficients and settling velocities of fractal aggregates, no single equation can best describe the settling behavior of fractal aggregates. The main reason for this is that it is extremely difficult to take into account the heterogeneous permeability and irregular shape of fractal aggregates. However, the evolution of the aggregate structure can be presented using the aggregate mass fractal dimension (D), and the aggregate effective density can be used to characterize the aggregate removal rates. Hence, the present study has involved measurement of the settling velocities for several aggregates within a glass-settling column and investigation of the relationship among the porosity, permeability, and settling velocity of asphaltene aggregates.

The simulation shows that the aggregate permeability is a strong function of the parameter d_p that is used. For the same d_p value, the permeability increased as the aggregate diameter increased, or increased at lower shear rates. However, large uncertainty may exist in such permeability estimation, because of assumptions used in d_p values. A direct and reliable method for permeability measurement is greatly needed.

Using the Brinkman permeability model, the size and settling-velocity measurements were used to compute the effective density of aggregates, as a function of aggregate size. The porosity of the aggregates is observed to increase with increases in their size. Higher porosity of the aggregates with an increasing characteristic length indicates that the structure of the aggregates possesses a space-filling capacity in which the nonsolid portion is relatively high, and the projected area is, therefore, not completely filled. This phenomenon is consistent with the smaller values of the experimentally observed three-dimensional (3-D) fractal dimensions ($D<2$). Within the data range of the present experimental study, the porosity was determined to be weakly dependent on the d_p values used. For the same size, the aggregates formed at different solid particle concentrations but at the same fluid shear rate exhibited almost the same porosity. For smaller aggregates, lower porosities were observed mostly at higher shear rates and are caused by their more-compact structures.

Although the density of aggregates with a diameter of >100 μm has almost the density of the liquid medium (i.e., very low effective density), they showed relatively high terminal settling velocities, because of their fractal structure, and very high porosity, which resulted in a significant reduction in the drag coefficient.

Acknowledgment. We would like to express our gratitude to the Alberta Department of Energy and Albian Sands Energy, Inc., for financial support of this project.

Nomenclature

A_{ns} = surface area of nonspherical particles (m^2)
A_s = surface area of spherical particles (m^2)
C_D = drag coefficient
D_3 = three-dimensional fractal dimension (also referenced as D)
d_a = aggregate projected area diameter (μm)
d_p = primary particle diameter (μm)
F_D = drag force (N)
g = acceleration due to gravity (m/s^2)
G_{avg} = volume averaged shear rate (s^{-1})
k = permeability (m^2)

(55) Ooms, G.; Mijnlieff, P. F.; Beckers, H. L. *J. Chem. Phys*. **1970**, *53*, 4123.
(56) Sutherland, D. N.; Tan, C. T. *Chem. Eng. Sci*. **1970**, *25*, 1948–1950.

K = resistance coefficient
l_a = aggregate longest dimension (μm)
n = number of spherical primary particles each of volume V_1 in the aggregate
N_{rps} = impeller rotational rate (rev/s)
p = fluid pressure (Pa)
Re = Reynolds number; Re = $Ud_a\rho_l/\mu$
Re_{imp} = impeller Reynolds number; $Re_{imp} = N_{rps}D_{imp}^2\rho/\mu$
Re_p = Reynolds number based on the primary particle and internal flow velocity through the pores; $Re_p = d_pU\rho_l/(\mu\epsilon)$
S_0 = specific surface area of the primary particle; $S_0 = 6/d_p$ (m^{-1})
t = time (s)
Δt = time interval
$\boldsymbol{u}$ = fluid velocity vector
U = settling velocity of a permeable aggregate (μm/s)
U_s = settling velocity predicted by Stokes' law (μm/s)
V_1 = volume of a spherical primary particle (μm^3)
V_a = aggregate volume (μm^3)

Greek

ϵ = porosity of the aggregates
μ = viscosity of the suspending liquid (Pa s)
ν = kinematic viscosity of the fluid (m^2/s)
ξ = energy dissipation rate per unit mass (m^2/s^3)
η = fluid collection efficiency
Ω = drag force factor or permeability correction factor
$\Gamma = 1/\Omega$.
β = normalized aggregate diameter or permeability factor
ψ = sphericity
ϕ = solid fraction of floc; $\phi = 1 - \epsilon$
$\gamma = \phi^{1/3}$
ρ_a = aggregate density (kg/m^3)
ρ_{eff} = aggregate effective density (kg/m^3)
ρ_l = density of the liquid (kg/m^3)
ρ_p = density of solid primary particle (kg/m^3)
ρ_s = dried solid density (kg/m^3)

EF0496707